

Critical Behaviour and Fractality in Shallow One-Dimensional Quasi-Periodic Potentials

Hepeng Yao, Alice Khoudli, Léa Bresque, and Laurent Sanchez-Palencia

CPHT, Ecole Polytechnique, CNRS, Institut Polytechnique de Paris, Route de Saclay, 91128 Palaiseau, France

(Dated: April 27, 2022)

Quasi-periodic systems offer an appealing intermediate between long-range ordered and genuine disordered systems, with unusual critical properties. One-dimensional models that break the so-called self-dual symmetry usually display a mobility edge, similarly as truly disordered systems in dimension strictly higher than two. Here, we determine the critical localization properties of single particles in shallow, one-dimensional, quasi-periodic models, and relate them to the fractal character of the energy spectrum. On the one hand, we determine the mobility edge and show that it separates the localized and extended phases, with no intermediate phase. On the other hand, we determine the critical potential amplitude and find the universal critical exponent $\nu \simeq 1/3$. We also study the spectral Hausdorff dimension and show that it is non-universal but always smaller than unity, hence showing that the spectrum is point-like. Finally, applications to on-going studies of Anderson localization, Bose glass physics, and many-body localization in ultracold atoms are discussed.

In an homogeneous system, all the single-particle wavefunctions are extended. In contrast, they may be exponentially localized in the presence of disorder owing to the breaking of translational invariance [1]. This effect, known as Anderson localization, is a fundamental, ubiquitous phenomenon at the origin of metal-insulator transitions in many systems [2]. Quasi-periodic models hold a special place for they are at the interface of long-range ordered and fully disordered systems. They describe a variety of systems, including quasicrystals [3], electronic materials in orthogonal magnetic fields [4–6] or with incommensurate charge-density waves [7], Fibonacci heterostructures [8], photonic crystals [9], and cavity polaritons [10]. They also proved pivotal in the context of disordered quantum gases [11–13] to investigate Anderson localization of matter waves [14–16] and interacting Bose gases [17], the emergence of long-range quasi-periodic order [18–20], Bose-glass physics [14, 15, 21–24], and many-body localization [25–28].

Anderson localization in quasi-periodic systems, however, significantly differ from its counterpart in truly disordered systems. For instance, while in a disordered system a phase transition between the Anderson-localized and extended phases occurs only in dimension strictly higher than 2 [29], it may occur in one-dimensional (1D) quasi-periodic systems. The most celebrated example is the Aubry-André (AA) model, obtained from the tight-binding model generated by a strong lattice, by adding a second, weak, incommensurate lattice. In the AA model, the localization transition occurs at a critical value of the quasi-periodic potential, irrespective of the particle energy [30]. This special behaviour results from a special symmetry of the AA model, known as self-duality. When the latter is broken, an energy mobility edge (ME), i.e. a critical energy separating localized and extended states, generally appears, as demonstrated in a variety of models [31–37]. One of the simplest examples is obtained by using two incommensurate lattices of comparable am-

plitudes. This model attracts significant attention in ultracold-atom systems [38, 39]. They have been used to study many-body localization in a 1D system exhibiting a single-particle ME [28] and may serve to overcome finite-temperature issues in the observation of the still elusive Bose-glass phase [24, 40] (see below). Recently, the localization properties and the ME of the single-particle problem have been studied both theoretically [39] and experimentally [41]. However, important critical properties of this model at still unknown. For instance, whether an intermediate phase appears in between the localized and extended phases remains unclear.

In this work, we study the critical properties and the fractality of non-interacting particles in shallow quasi-periodic potentials. We consider various models, including bichromatic and trichromatic lattices with balanced and imbalanced amplitudes. In all cases, above a certain critical amplitude of the quasi-periodic potential V_c , we find a finite energy ME. It marks a sharp transition between the localized and extended phases with no intermediate phase. The ME is always found in one of the energy band gaps, which are dense. We show that this is a direct consequence of the fractal, point-like, character of the energy spectrum. We compute the critical Hausdorff dimension and find values significantly different from that found for the AA model. Moreover, we determine accurate values of the critical quasi-periodic amplitude V_c from the scaling of the inverse participation ratio. While V_c depends on the model, we find the universal critical exponent $\nu \simeq 1/3$.

Model and approach.— The single-particle wavefunctions $\psi(x)$ are found by solving numerically the continuous-space, 1D Schrödinger equation,

$$E\psi(x) = -\frac{\hbar^2}{2m} \frac{d^2\psi}{dx^2} + V(x)\psi(x), \quad (1)$$

using exact diagonalization for Dirichlet absorbing boundary conditions, $\psi_n(0) = \psi_n(L) = 0$. Here, E and

m are the particle energy and mass, L is the system size, and \hbar is the reduced Planck constant. In the first part of this work, we consider the bichromatic lattice potential

$$V(x) = \frac{V_1}{2} \cos(2k_1x) + \frac{V_2}{2} \cos(2k_2x + \varphi), \quad (2)$$

where the quantities V_j ($j = 1, 2$) are the amplitudes of two periodic potentials of incommensurate spatial periods π/k_j with $k_2/k_1 = r$, an irrational number. The relative phase shift φ is essentially irrelevant, except for special values, which induce special symmetries. In the following, we use $r = (\sqrt{5}-1)/2$ and $\varphi = 4$, which avoids such cases. We then characterize the localization of an eigenstate ψ using the 2nd order inverse participation ratio (IPR) [42],

$$\text{IPR} = \frac{\int dx |\psi_n(x)|^4}{\left(\int dx |\psi_n(x)|^2\right)^2}. \quad (3)$$

It generally scales as $\text{IPR} \sim 1/L^\tau$, with $\tau = 1$ for an extended state and $\tau = 0$ for a localized state.

Mobility edge.— We first focus on the balanced bichromatic lattice, Eq. (2) with $V_1 = V_2 \equiv V$. Note that this model cannot be mapped onto the AA model, even for $V \gg E_r$, where $E_r = \hbar^2 k_1^2 / 2m$ is the recoil energy, since none of the periodic components of $V(x)$ dominates the other. Figure 1(a) shows the IPR versus the particle energy E and the potential amplitude V for a large system, $L = 100a$ with $a = \pi/k_1$ the spatial period of the first periodic potential. The results indicate the onset of localization (corresponding to large values of the IPR) at low particle energy and high potential amplitude, consistently with the existence of a V -dependent energy ME E_c . This is confirmed by the behaviour of the wavefunctions, which turn from exponentially localized at low energy [Figs. 1(b)] to extended at high energy [Figs. 1(c)]. These results are characteristic of 1D quasi-periodic models that break the AA self-duality condition [34, 38, 39]. The IPR, however, varies smoothly with the particle energy, and is not sufficient to distinguish extended states from states localized on a large scale.

To determine the ME precisely, we perform a systematic finite-size scaling analysis of the IPR and compute the quantity

$$\tau(L) \equiv -d \log \text{IPR} / d \log L. \quad (4)$$

For all values of V and E , and for large enough system lengths, we find either $\tau = 0 \pm 0.2$ or $\tau = 1 \pm 0.2$ [43]. It shows the existence of a sharp localization transition (ME) between bands of localized states ($\tau \simeq 0$) at low energy and bands of extended states ($\tau \simeq 1$) at high energy. No intermediate behaviour is found in the thermodynamic limit. The ME E_c is then accurately determined as the energy of the transition point between the two values.

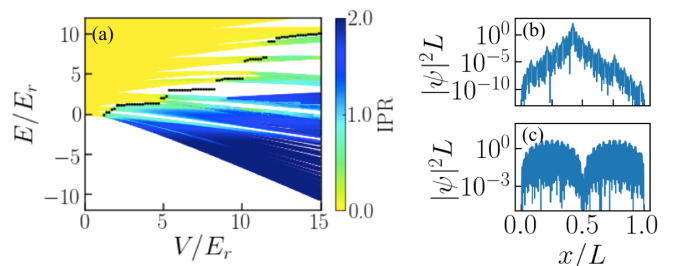


Figure 1. Localization transition for the balanced bichromatic potential, Eq. (2) with $V_1 = V_2 \equiv V$. (a) IPR versus the particle energy E and the lattice amplitude V for the system size $L = 100a$. Localized states correspond to large values of the IPR (blue) and extended to vanishingly small values (yellow). The ME, found from finite- L scaling analysis of the IPR, is shown as black points. (b) and (c) Density profiles of two eigenstates in the localized and extended regimes respectively. Here, the two states correspond to energies right below and right above the ME at $V = 2E_r$.

The results are plotted on Fig. 1(a) (black dots). In all cases, we find that the ME is in an energy band gap. While it is clearly seen for some potential amplitudes (e.g. for $5.2 \lesssim V \lesssim 8.5$), it is more elusive for some other values (e.g. for $V/E_r \gtrsim 8.5$), see Fig. 1(a). In the latter case, however, it can be seen by zooming in the figure. More fundamentally, it is a direct consequence of the fractal behaviour of the energy spectrum, as we discuss now.

Fractality and point-like spectrum.— To characterize the energy spectrum, we first compute the integrated density of states (IDOS) per unit lattice spacing $n_\epsilon(E)$, i.e. the number of eigenstates in the energy range $[E - \epsilon/2, E + \epsilon/2]$, divided by L/a . Figures 2(a) and (b) show the quantity $n_\epsilon(E)/\epsilon$ in the vicinity of the ME for two values of the quasi-periodic amplitude V and several energy resolutions ϵ [44]. For any value of ϵ , the IDOS displays energy bands separated by gaps. However, when the resolution ϵ decreases (corresponding to increasingly dark lines on the plots), new gaps appear inside the bands, while the existing gaps are stable. It signals that the spectrum is point like while the gaps are dense in the thermodynamic limit. In particular, the density of states, $\lim_{\epsilon \rightarrow 0+} n_\epsilon(E)/\epsilon$, is singular. Moreover, the ME is always found in a gap for a sufficiently resolved spectrum, see Figs. 2(a) and (b). Note that this is not a finite-size effect: For all the results shown here, we have used large enough systems so that each ϵ -resolved band contains at least 10 to 15 states. In addition, we have checked that the IDOS is stable against further increasing the system's length [43]. The opening of an infinite series of mini-gaps is characteristic of a fractal behaviour.

So far, the fractal character of the energy spectrum of 1D incommensurate systems has been studied for discrete models, such as the Fibonacci chain and the AA model [6, 10, 45–48]. It was shown that in these cases

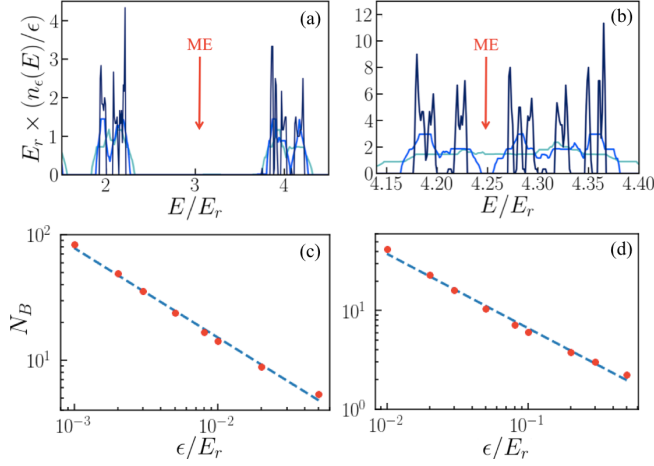


Figure 2. Fractal behaviour of the energy spectrum. Panel (a) shows $n_\epsilon(E)/\epsilon$ in the vicinity of the ME at $V = 6.0E_r$ for $L = 600a$ and $\epsilon/E_r = 0.1$ (light blue), 0.05 (blue), 0.01 (dark blue). Panel (b) shows the same quantity for the ME at $V = 8.5E_r$ for $L = 1000a$ and $\epsilon/E_r = 0.1$ (light blue), 0.03 (blue), 0.003 (dark blue). Panels (c) and (d) show the energy-box counting number N_B versus ϵ for the parameters of (a) and (b), respectively. The linear slopes in log-log scale are consistent with a fractal behaviour, Eq. (6), with $D_H = 0.72 \pm 0.03$ and $D_H = 0.76 \pm 0.03$, respectively.

the spectrum is homeomorphic to Cantor sets. To study fractality in our continuous model, we use a direct box-counting analysis [49, 50]: We introduce the *energy-box counting number*,

$$N_B(\epsilon) = \lim_{q \rightarrow 0+} \int_{E_1}^{E_2} \frac{dE}{\epsilon} [n_\epsilon(E)]^q, \quad (5)$$

for some energy range $[E_1, E_2]$. In the limit $q \rightarrow 0+$, the quantity $[n_\epsilon(E)]^q$ approaches 1 if $n_\epsilon(E) \neq 0$ and 0 if $n_\epsilon(E) = 0$. Therefore, the quantity $\lim_{q \rightarrow 0+} [n_\epsilon(E)]^q$ contributes 1 in the boxes of width ϵ containing at least one state and vanishes in the empty boxes. The sum of these contributions, $N_B(\epsilon)$, counts the minimal number of ϵ -wide boxes necessary to cover all the states within the energy range $[E_1, E_2]$. The scaling of $N_B(\epsilon)$ versus the energy resolution ϵ ,

$$N_B(\epsilon) \sim \epsilon^{-D_H}, \quad (6)$$

defines the Hausdorff dimension D_H of the energy spectrum. In all considered cases, we found a scaling consistent with Eq. (6) with $0 < D_H < 1$. This is characteristic of a non-trivial fractal behaviour [51]. For instance Figs. 2(c) and (d) show N_B versus ϵ in the vicinity of the MEs at $V = 6E_r$ and $V = 8.5E_r$ for the energy ranges corresponding to Figs. 2(a) and (b), respectively. We find a linear scaling in log-log scale, consistent with Eq. (6) and the Hausdorff dimensions $D_H = 0.72 \pm 0.03$ and $D_H = 0.76 \pm 0.03$, respectively. Both values are significantly smaller than the geometrical dimension $d = 1$.

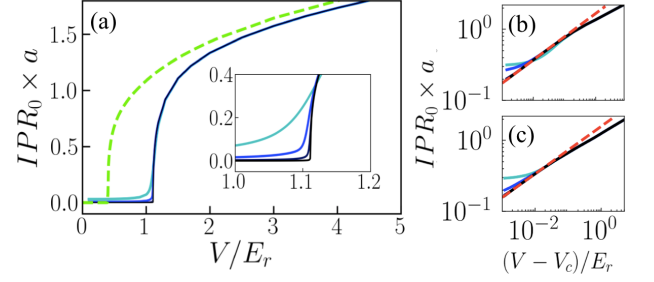


Figure 3. Critical localization behaviour. (a) IPR of the ground state versus the quasi-periodic amplitude for the balanced bichromatic lattice (solid lines). The inset shows a magnification in the vicinity of the critical point at V_c . Darker lines correspond to increasing system sizes, $L/a = 50$ (light blue), 200 (blue), 1000 (dark blue), 10000 (black). The dashed green line corresponds to the trichromatic lattice for $L/a = 10000$. (b) and (c) IPR of the ground state versus $V - V_c$ in log-log scale for the bichromatic and trichromatic lattices, respectively.

Therefore, the Lebesgue measure of the energy support vanishes and the spectrum is nowhere dense in the thermodynamic limit.

Note that the Hausdorff dimension found above significantly differs from that found in previous work at the critical point of the AA model, $D_H \simeq 0.5$ [46, 47]. We conclude that the spectral Hausdorff dimension is a non-universal quantity. This is confirmed by further calculations we performed. For instance, in the AA limit of our continuous model, $V_1 \gg V_2, E_r$, we recover $D_H = 0.507 \pm 0.005$ at the critical point. Conversely, we found $D_H = 0.605 \pm 0.014$ at the critical point of the balanced lattice (see below).

Criticality.— We now turn to the critical localization behaviour. As shown on Fig. 1(a), a finite ME appears only for a potential amplitude V larger than some critical value V_c , see also Ref. [34]. On Fig. 3(a), we plot the IPR of the ground state (IPR_0) versus V . The transition from the extended phase (vanishingly small IPR) to the localized phase (finite IPR) gets sharper when the system size increases, and becomes critical in the thermodynamic limit (see darker solid blue lines in the main figure and the inset). Since the IPR scales as $IPR_0 \sim 1/L$ in the extended phase and as $IPR_0 \sim 1$ in the localized phase, the critical amplitude can be found with a high precision as the fixed point of $IPR_0 \times \sqrt{La}$ when increasing the system size L . It yields [43]

$$V_c/E_r \simeq 1.112 \pm 0.002. \quad (7)$$

Furthermore, this accurate value of V_c allows us to determine the critical exponent of the transition. Plotting IPR_0 versus $V - V_c$ in log-log scale, we find a clear linear behaviour for sufficiently large systems, consistently with the power-law scaling $IPR_0 \sim (V - V_c)^\nu$, see Fig. 3(b). Fitting the slope, we find the critical ex-

ponent $\nu \simeq 0.327 \pm 0.007$. Note that for $V \gg V_c$, E_r , the behaviour of the IPR changes and we find the scaling $\text{IPR}_0 \sim V^{\nu'}$ with $\nu' \simeq 0.258 \pm 0.005$. This is consistent with the exponent $1/4$ expected in the tight-binding limit [43].

Other quasi-periodic lattices and universality.— We now extend our results to other quasi-periodic models. We first consider the imbalanced bichromatic lattice, Eq. (2) with $V_1 \neq V_2$. On Fig. 4, we plot the ME versus the quasi-periodic amplitudes V_1 and V_2 . The dark region corresponds to cases where the ME is absent. Its boundary yields the critical line in the plan V_1 - V_2 . For $V_1 = V_2$, we recover the ME given in Eq. (7). For $V_1 \gg V_2$, E_r (resp. $V_2 \gg V_1$, E_r), the critical point is consistent with the AA result $\Delta = 2J$ [30], where J is the tunneling energy induced by lattice 1 (resp. 2) and Δ is the quasi-periodic amplitude associated to lattice 2 (resp. 1) [43]. Note that Fig 4 is not symmetric by exchange of V_1 and V_2 even upon rescaling the energies. This owns to the strong dependence of the model on the incommensurate ratio r . However, we found that the localization transition is universal. Scanning V_1 up to values deep in the AA limit ($50E_r$), as well as for the discrete AA model, we always find $\text{IPR}_0 \sim (V_2 - V_{2c})^\nu$ with $\nu \simeq 0.33 \pm 0.02$ [43].

It is worth noting that the behaviour of the IPR differs from that of the Lyapunov exponent (inverse localization length). The IPR is dominated by the core of the wavefunction and characterizes for instance the short-range interaction energy of two particles in a localized state [52]. In contrast, the Lyapunov exponent γ characterizes the exponential tails of the wavefunctions, $\psi(x) \sim \exp(-\gamma|x|)$, and is insensitive to the core. For non-purely exponential wavefunctions, which appear in our model (see for instance Fig. 1(b) and Ref. [43]), these two quantities are not proportional. For instance, in the AA model, we have $\gamma \sim \ln(\Delta/2J)$, and, at the critical point $\Delta = 2J$, one finds $\gamma \sim \Delta/2J \sim (V_2 - V_{2c})^\beta$ with the Lyapunov critical exponent $\beta = 1$. This value differs from the IPR critical exponent, $\nu \simeq 1/3$, found above.

We also considered the trichromatic lattice

$$V(x) = \frac{V}{2} [\cos(2k_1x) + \cos(2k_2x + \varphi) + \cos(2k_3x + \varphi')], \quad (8)$$

with $k_3/k_2 = k_2/k_1 = r$, so that the three lattice spacings are incommensurate to each other [note that $k_3/k_1 = r^2 = (3 - \sqrt{5})/2$ is an irrational number]. Performing the same analysis as for the other models, we recover the same universal features. In particular, the energy spectrum is fractal and nowhere dense, and the mobility edge is always in a gap. We find a finite critical amplitude V_c and the critical behaviour $\text{IPR}_0 \sim (V - V_c)^\nu$ with $\nu \simeq 0.327 \pm 0.007$, see Fig 3(c). The only significant difference is that the critical point for the trichromatic lattice, $V_c/E_r \simeq 0.400 \pm 0.005$, is smaller than for the bichromatic lattice, see Fig. 3(a). In particular, the standard deviation of the potential, ΔV , is a factor about

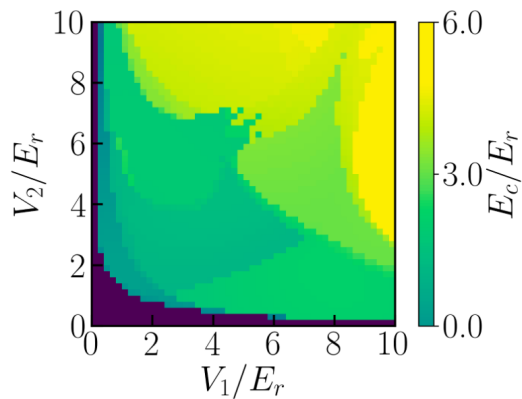


Figure 4. Mobility edge for the imbalanced bichromatic lattice, Eq. (2) versus the amplitudes V_1 and V_2 . The dark region indicates the absence of a mobility edge, and its boundary the localization critical line.

2.27 smaller at the critical point. This is consistent with the intuitive expectation that it should vanish in the disordered case corresponding to an infinite series of cosine components with random phases [53, 54].

Conclusion.— In summary, we have studied the critical properties and the fractal behaviour for single particles in quasi-periodic potentials. On the one hand, our results shed light on models that have become pivotal for the study of Anderson [39, 41] and many-body [28] localization. In particular, we found that the ME is always in a gap and separates the localized and extended phases, with no intermediate phase. We related this behaviour to the fractal structure of the energy spectrum and found that the Hausdorff dimension is always smaller than unity but non-universal. In contrast, we found the critical behaviour $\text{IPR}_0 \sim (V - V_c)^\nu$ with the universal exponent $\nu \simeq 1/3$. These predictions may be directly confirmed in experiments such as that of Ref. [41] using energy-resolved selection of states [55–57] for instance. In parallel to further theoretical studies, they may help answering questions our results call. For instance, it would be interesting to determine the physical origin of the critical exponent ν and extend our study to higher dimensions. Another important avenue would be to extend it to interacting models in connection to many-body localization.

On the other hand, our results may pave the way to the observation of the still elusive Bose glass phase. So far experiments with ultracold atoms have been performed only in the AA limit, the energy scale of which is the tunneling energy J . The latter is exponentially small in the amplitude of the main lattice and of the order of the temperature, which thus significantly alters the phase diagram [24, 40]. In shallow quasi-periodic potentials as considered here, the energy scale is, instead, the recoil energy E_r , which is much higher than the temperature. Temperature effects should thus be negligible.

We thank David Clément and Thierry Giamarchi for fruitful discussions. This research was supported by the European Commission FET-Proactive QUIC (H2020 grant No. 641122) and the Paris region DIM-SIRTEQ. This work was performed using HPC resources from GENCI-CINES (Grant 2018-A0050510300). We thank the CPHT computer team for valuable support.

-
- [1] P. W. Anderson, *Absence of diffusion in certain random lattices*, Phys. Rev. **109**, 1492 (1958).
 - [2] E. Abrahams, *50 years of Anderson Localization* (World Scientific, Singapore, 2010).
 - [3] D. Shechtman, I. Blech, D. Gratias, and J. W. Cahn, *Metallic phase with long-range orientational order and no translational symmetry*, Phys. Rev. Lett. **53**, 1951 (1984).
 - [4] R. Peierls, *Theory of the diamagnetism of conduction electrons*, Z. Phys. **80**, 763 (1933).
 - [5] P. G. Harper, *Single band motion of conduction electrons in a uniform magnetic field*, Proc. Phys. Soc. London **A 68**, 874 (1955).
 - [6] D. R. Hofstadter, *Energy levels and wave functions of Bloch electrons in rational and irrational magnetic fields*, Phys. Rev. B **14**, 2239 (1976).
 - [7] J. Wilson, F. Di Salvo, and S. Mahajan, *Charge-density waves and superlattices in the metallic layered transition metal dichalcogenides*, Adv. Phys. **24**, 117 (1975).
 - [8] R. Merlin, K. Bajema, R. Clarke, F. Y. Juang, and P. K. Bhattacharya, *Quasiperiodic GaAs-AlAs heterostructures*, Phys. Rev. Lett. **55**, 1768 (1985).
 - [9] Y. Lahini, R. Pugatch, F. Pozzi, M. Sorel, R. Morandotti, N. Davidson, and Y. Silberberg, *Observation of a localization transition in quasiperiodic photonic lattices*, Phys. Rev. Lett. **103**, 013901 (2009).
 - [10] D. Tanese, E. Gurevich, F. Baboux, T. Jacqmin, A. Lemaître, E. Galopin, I. Sagnes, A. Amo, J. Bloch, and E. Akkermans, *Fractal energy spectrum of a polariton gas in a Fibonacci quasiperiodic potential*, Phys. Rev. Lett. **112**, 146404 (2014).
 - [11] A. Aspect and M. Inguscio, *Anderson localization of ultracold atoms*, Phys. Today **62**, 30 (2009).
 - [12] G. Modugno, *Anderson localization in Bose-Einstein condensates*, Rep. Prog. Phys. **73**, 102401 (2010).
 - [13] L. Sanchez-Palencia and M. Lewenstein, *Disordered quantum gases under control*, Nat. Phys. **6**, 87 (2010).
 - [14] B. Damski, J. Zakrzewski, L. Santos, P. Zoller, and M. Lewenstein, *Atomic Bose and Anderson glasses in optical lattices*, Phys. Rev. Lett. **91**, 080403 (2003).
 - [15] R. Roth and K. Burnett, *Phase diagram of bosonic atoms in two-color superlattices*, Phys. Rev. A **68**, 023604 (2003).
 - [16] G. Roati, F. Riboli, G. Modugno, and M. Inguscio, *Fermi-Bose quantum degenerate ^{40}K - ^{87}Rb mixture with attractive interaction*, Phys. Rev. Lett. **89**, 150403 (2002).
 - [17] S. Lellouch and L. Sanchez-Palencia, *Localization transition in weakly-interacting Bose superfluids in one-dimensional quasiperiodic lattices*, Phys. Rev. A **90**, 061602(R) (2014).
 - [18] L. Sanchez-Palencia and L. Santos, *Bose-Einstein condensates in optical quasicrystal lattices*, Phys. Rev. A **72**, 053607 (2005).
 - [19] N. Macé, A. Jagannathan, and M. Duneau, *Quantum simulation of a 2D quasicrystal with cold atoms*, Crystals **6**, 124 (2016).
 - [20] K. Viebahn, M. Sbroscia, E. Carter, C. Yu Jr, and U. Schneider, *Matter-wave diffraction from a quasicrystalline optical lattice*, arXiv:1807.00823 (2018).
 - [21] L. Fallani, J. E. Lye, V. Guarrera, C. Fort, and M. Inguscio, *Ultracold atoms in a disordered crystal of light: Towards a Bose glass*, Phys. Rev. Lett. **98**, 130404 (2007).
 - [22] B. Gadway, D. Pertot, J. Reeves, M. Vogt, and D. Schneble, *Glassy behavior in a binary atomic mixture*, Phys. Rev. Lett. **107**, 145306 (2011).
 - [23] L. Tanzi, E. Lucioni, S. Chaudhuri, L. Gori, A. Kumar, C. D'Errico, M. Inguscio, and G. Modugno, *Transport of a Bose gas in 1D disordered lattices at the fluid-insulator transition*, Phys. Rev. Lett. **111**, 115301 (2013).
 - [24] C. D'Errico, E. Lucioni, L. Tanzi, L. Gori, G. Roux, I. P. McCulloch, T. Giamarchi, M. Inguscio, and G. Modugno, *Observation of a disordered bosonic insulator from weak to strong interactions*, Phys. Rev. Lett. **113**, 095301 (2014).
 - [25] S. Iyer, V. Oganesyan, G. Refael, and D. A. Huse, *Many-body localization in a quasiperiodic system*, Phys. Rev. B **87**, 134202 (2013).
 - [26] A. Lukin, M. Rispoli, R. Schittko, M. E. Tai, A. M. Kaufman, S. Choi, V. Khemani, J. Léonard, and M. Greiner, *Probing entanglement in a many-body-localized system*, arXiv preprint arXiv:1805.09819 (2018).
 - [27] R. Matthew, L. Alexander, S. Robert, K. Sooshin, T. M. Eric, L. Julian, and G. Markus, *Quantum critical behavior at the many-body-localization transition*, arXiv preprint arXiv:1812.06959 (2018).
 - [28] T. Kohlert, S. Scherg, X. Li, H. P. Lüschen, S. D. Sarma, I. Bloch, and M. Aidelsburger, *Observation of many-body localization in a one-dimensional system with single-particle mobility edge*, arXiv:1809.04055 (2018).
 - [29] E. Abrahams, P. W. Anderson, D. C. Licciardello, and T. V. Ramakrishnan, *Scaling theory of localization: Absence of quantum diffusion in two dimensions*, Phys. Rev. Lett. **42**, 673 (1979).
 - [30] S. Aubry and G. André, *Analyticity breaking and Anderson localization in incommensurate lattices*, Ann. Israel Phys. Soc. **3**, 133 (1980).
 - [31] C.M. Soukoulis and E.N. Economou, *Localization in one-dimensional lattices in the presence of incommensurate potentials*, Phys. Rev. Lett. **48**, 1043 (1982).
 - [32] S. Das Sarma, A. Kobayashi, and R. E. Prange, *Proposed experimental realization of Anderson localization in random and incommensurate artificially layered systems*, Phys. Rev. Lett. **56**, 1280 (1986).
 - [33] S. Das Sarma, S. He, and X.C. Xie, *Mobility edge in a model one-dimensional potential*, Phys. Rev. B **41**, 5544 (1990).
 - [34] J. Biddle, B. Wang, D. J. Priour Jr, and S. Das Sarma, *Localization in one-dimensional incommensurate lattices beyond the Aubry-André model*, Phys. Rev. A **80**, 021603(R) (2009).
 - [35] J. Biddle and S. Das Sarma, *Predicted mobility edges in one-dimensional incommensurate optical lattices: An exactly solvable model of anderson localization*, Phys. Rev. Lett. **104**(7), 070601 (2010).
 - [36] J. Biddle, D. J. Priour Jr, B. Wang, and S. Das Sarma,

- Localization in one-dimensional lattices with non-nearest-neighbor hopping : Generalized Anderson and Aubry-André models*, Phys. Rev. B **83**, 075105 (2011).
- [37] S. Ganeshan, J.H. Pixley, and S. Das Sarma, *Nearest neighbor tight binding models with an exact mobility edge in one dimension*, Phys. Rev. Lett. **114**, 146601 (2015).
- [38] D. J. Boers, B. Goedeke, D. Hinrichs, and M. Holthaus, *Mobility edges in bichromatic optical lattices*, Phys. Rev. A **75**, 063404 (2007).
- [39] X. Li, X. Li, and S. Das Sarma, *Mobility edges in one-dimensional bichromatic incommensurate potentials*, Phys. Rev. B **96**, 085119 (2017).
- [40] L. Gori, T. Barthel, A. Kumar, E. Lucioni, L. Tanzi, M. Inguscio, G. Modugno, T. Giamarchi, C. D’Errico, and G. Roux, *Finite-temperature effects on interacting bosonic one-dimensional systems in disordered lattices*, Phys. Rev. A **93**, 033650 (2016).
- [41] H. P. Lüschen, S. Scherg, T. Kohlert, M. Schreiber, P. Bordia, X. Li, S. Das Sarma, and I. Bloch, *Single-particle mobility edge in a one-dimensional quasiperiodic optical lattice*, Phys. Rev. Lett. **120**, 160404 (2018).
- [42] F. Evers and A. D. Mirlin, *Anderson transitions*, Rev. Mod. Phys. **80**, 1355 (2008).
- [43] For details, see Supplemental Material. It discusses the scaling analyses of the IPR and IDOS, the determination of the critical point V_c , the critical behaviour for the imbalanced bichromatic lattice, and the tight-binding and AA limits.
- [44] The quantity $n_\epsilon(E)/\epsilon$ may be interpreted as the density of states (DOS) for an energy resolution ϵ . Due to the fractality of the energy spectrum, the DOS, $\lim_{\epsilon \rightarrow 0+} n_\epsilon(E)/\epsilon$, is, however, ill defined (see below).
- [45] M. Kohmoto, *Metal-insulator transition and scaling for incommensurate systems*, Phys. Rev. Lett. **51**, 1198 (1983).
- [46] C. Tang and M. Kohmoto, *Global scaling properties of the spectrum for a quasiperiodic Schrödinger equation*, Phys. Rev. B **34**, 2041 (1986).
- [47] M. Kohmoto, B. Sutherland, and C. Tang, *Critical wave functions and a Cantor-set spectrum of a one-dimensional quasicrystal model*, Phys. Rev. B **35**, 1020 (1987).
- [48] T. Roscilde, *Bosons in one-dimensional incommensurate superlattices*, Phys. Rev. A **77**, 063605 (2008).
- [49] B. B. Mandelbrot, *The Fractal Geometry of Nature*, vol. 2 (WH freeman New York, 1982).
- [50] J. Theiler, *Estimating fractal dimension*, JOSA A **7**, 1055 (1990).
- [51] For a continuous (resp. discrete) spectrum, one finds $D_H = 1$ (resp. 0). Intermediate values of D_H are characteristic of a non-trivial self-similar behaviour.
- [52] P. Lugan, D. Clément, P. Bouyer, A. Aspect, M. Lewenstein, and L. Sanchez-Palencia, *Ultracold Bose gases in 1D disorder: From Lifshits glass to Bose-Einstein condensate*, Phys. Rev. Lett. **98**, 170403 (2007).
- [53] I. M. Lifshits, S. Gredeskul, and L. Pastur, *Introduction to the Theory of Disordered Systems* (Wiley, New York, 1988).
- [54] C. W. J. Beenakker, *Random-matrix theory of quantum transport*, Rev. Mod. Phys. **69**, 731 (1997).
- [55] L. Pezzé and L. Sanchez-Palencia, *Localized and extended states in a disordered trap*, Phys. Rev. Lett. **106**, 040601 (2011).
- [56] V. V. Volchkov, M. Pasek, V. Denechaud, M. Mukhtar, A. Aspect, D. Delande, and V. Josse, *Measurement of spectral functions of ultracold atoms in disordered potentials*, Phys. Rev. Lett. **120**, 060404 (2018).
- [57] J. Richard, L.-K. Lim, V. Denechaud, V. V. Volchkov, B. Lecoutre, M. Mukhtar, F. Jendrzejewski, A. Aspect, A. Signoles, L. Sanchez-Palencia, *et al.*, *Elastic scattering time of matter waves in disordered potentials*, Phys. Rev. Lett. **122**, 100403 (2019).

Supplemental Material for

Critical Behaviour and Fractality in Shallow One-Dimensional Quasi-Periodic Potentials

This supplemental material gives details about the finite-size scaling analyses used for the mobility edge, the integrated density of states, and the critical point (Sec. S1), as well as about the tight-binding and AA limits (Sec. S2).

S1. FINITE-SIZE SCALING ANALYSES

Here we discuss the finite-size scaling analyses performed for the determination of the mobility edge (Sec. S1 A), the fractal, point-like character of the energy spectrum (Sec. S1 B), and the critical potential amplitude (Sec. S1 C).

A. Inverse participation ratio

The scaling analysis of the inverse participation ratio (IPR) is performed as follows. For each value of the quasi-periodic amplitude V , we diagonalize the Hamiltonian for a series of system sizes L , typically ranging from $50a$ to $800a$ (a is the spacing of the first lattice). For any state, we find that the IPR scales as $\text{IPR} \sim L^\tau$, with either $\tau = 0 \pm 0.2$ or $\tau = 1 \pm 0.2$. Therefore, in contrast to the IPR at a given system length, which varies smoothly [see Fig. 1(a) of the main paper, also reproduced on Fig. S1(a)], the exponent τ shows a sharp transition from localized states (corresponding to $\tau \simeq 0$) to extended states (corresponding to $\tau \simeq 1$), see Fig. S1(b) as well as Fig. S1(c) and (d) for two typical cuts at fixed values of the quasi-periodic amplitude. The mobility edge (ME) E_c is then determined as the transition point between the values of τ , see black points on Fig. S1(b). More precisely, as discussed in the main paper, the ME is always in an energy gap and we define E_c as the average energy of the last localized state and the first extended state, see dashed black lines on Figs. S1(c) and (d), corresponding to a large and small gap, respectively.

B. Integrated density of states

To show that the opening of mini gaps in the energy spectrum is not due to finite-size effects, we have computed the integrated density of states (IDOS) for various system lengths. Fig. S2 reproduces the IDOS shown on Fig. 2 of the main paper for the smallest considered energy resolutions ϵ and various values of the length L . For both Figs. S2(a) and (b), the results corresponding to different lengths are indistinguishable. The computed IDOS is thus stable against increasing the system's length, which rules out finite-size effects. Moreover, the computed IDOS are all smooth functions of the energy E . It confirms that the lengths we use are sufficiently large for the considered energy resolutions ϵ . Note that larger lengths are necessary for smaller energy resolutions.

C. Determination of the critical potential

Figure S3 shows the determination of the critical potential amplitude V_c for the balanced bichromatic lattice. We compute the ground-state IPR rescaled by square root of the dimensionless length, $\text{IPR}_0 \times \sqrt{La}$ as a function of V . In the extended phase, it scales as $\text{IPR}_0 \times \sqrt{La} \sim 1/\sqrt{L}$ and is thus vanishingly small. Conversely, it scales as $\text{IPR}_0 \times \sqrt{La} \sim \sqrt{L}$ in the localized phase and thus diverges with the system length. The critical potential amplitude V_c is then determined as the turning point. For large enough systems, the curves corresponding to different lengths cross each other approximately at the same value of V/E_r . It yields an accurate estimate of the critical point, $V_c/E_r \simeq 1.112 \pm 0.002$ [Eq. (7) of the main paper].

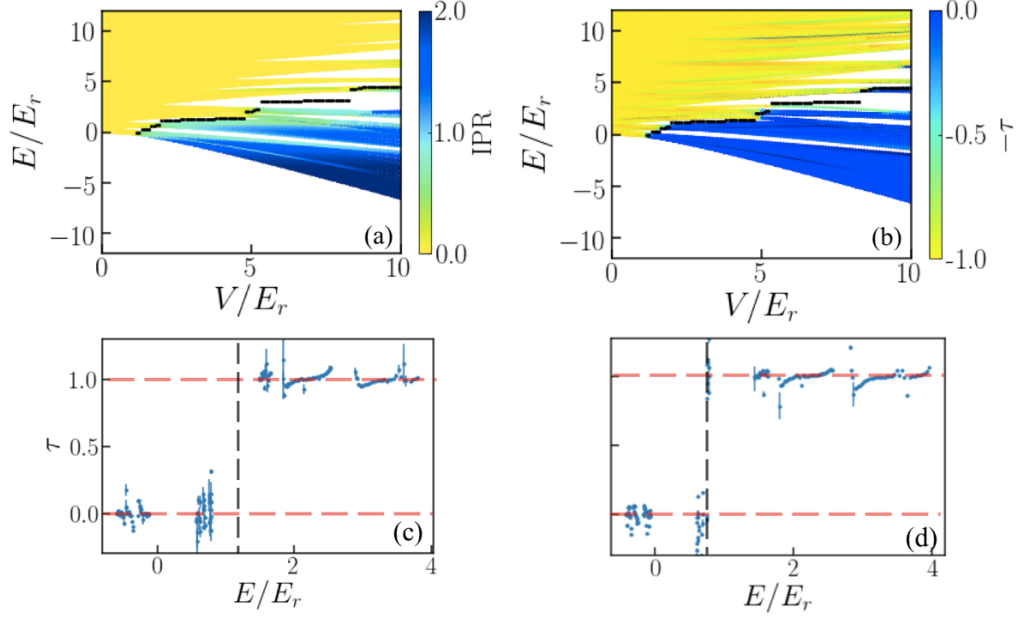


Figure S1. Accurate determination of the energy mobility edge E_c for the balanced bichromatic lattice. Panel (a) shows the IPR versus the particle energy E and the lattice amplitude V for the system size $L = 100a$ [reproduced from Fig. 1(a) of the main paper]. Panel (b) shows the exponent τ versus E and V , as found from finite-size scaling analysis of data computed for various system sizes. Panels (c) and (d) are cuts of panel (b) at $V = 2E_r$ and $V = 1.7E_r$, respectively. The system size ranges from $L = 50a$ to $L = 800a$ for most of the points. When the ME lies in a very small gap, as for panel (d) for instance we use larger system sizes, typically up to $L = 1000a$.

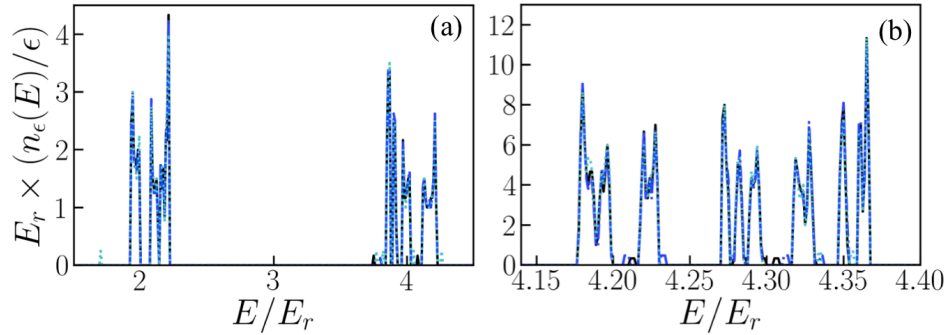


Figure S2. Finite-size scaling analysis for the IDOS. The figure reproduces the IDOS divided by the energy resolution, $n_\epsilon(E)/\epsilon$, shown on Fig. 2 of the main paper for the smallest considered energy resolutions ϵ but for various values of the length L . (a) IDOS in the vicinity of the ME at $V = 6E_r$ for $\epsilon = 0.01E_r$ and $L = 400a$ (dotted light blue line), $600a$ (dashed blue line), $800a$ (solid black line). (b) Same as panel (a) for $V = 8.5E_r$, $\epsilon = 0.003E_r$, and $L = 800a$ (dotted light blue line), $1000a$ (dashed blue line), $1200a$ (solid black line).

S2. TIGHT-BINDING LIMIT AND AUBRY-ANDRÉ MODEL

A. Inverse participation ratio of the ground state in deep lattices

The tight-binding limit is obtained when at least one of the potential amplitudes exceeds the recoil energy, $V_j \gg E_r$. In this case, the local potential minima support bound states and, for the quasi-periodic potential, the tunneling is suppressed. Within a harmonic approximation of the potential minima, we find the frequency $\omega \propto \sqrt{VE_r}/\hbar$. The ground state and, more generally, the lowest energy eigenstates of the quasi-periodic potential are Gaussian functions of width $\ell = \sqrt{\hbar/m\omega}$ and centered at the bottom of different potential minima. Then, the IPR of the ground state

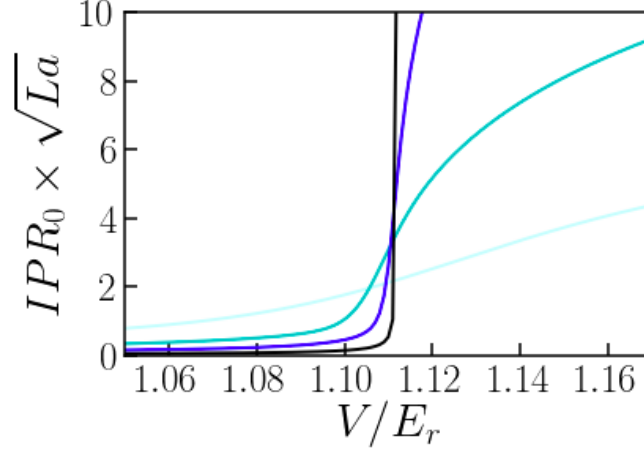


Figure S3. Finite-size scaling determination of the critical potential amplitude V_c for the balanced bichromatic lattice. The figure shows the rescaled IPR of the ground state, $IPR_0 \times \sqrt{La}$, as a function of the potential amplitude V for $L = 50a$ (light blue line), $200a$ (blue line), $1000a$ (dark blue line), $1000a$ (dark blue line), $L = 10000a$ (black line).

scales as $IPR_0 \sim 1/\ell$, i.e.

$$IPR_0 \sim V^{\nu'} \quad \text{with} \quad \nu' = 1/4. \quad (S1)$$

This exponent differs significantly from the critical exponent $\nu \simeq 1/3$ found at the critical point V_c .

B. Aubry-André model

The Aubry-André (AA) limit of our continuous bichromatic lattice is found in the tight-binding limit of one of the lattices (say lattice 1) with the other lattice (say lattice 2) is weak. Our model can then be mapped onto the discrete, Aubry-André model,

$$\hat{H}_{AA} = -J \sum_{\langle i,j \rangle} (\hat{a}_i^\dagger \hat{a}_j + \text{H.c.}) + \Delta \sum_i \cos(2\pi r i + \varphi) \hat{a}_i^\dagger \hat{a}_i, \quad (S2)$$

where \hat{a}_i is the annihilation operator of a particle in the lattice site i (located at the position $x_i = a \times i$), J is the tunneling energy associated to the lattice 1 and Δ is the quasi-periodic amplitude induced by the lattice 2. The latter are given by

$$J \simeq \frac{4E_r}{\sqrt{\pi}} \left(\frac{V_1}{E_r} \right)^{3/4} \exp \left(-2\sqrt{\frac{V_1}{E_r}} \right) \quad \text{with} \quad \Delta \simeq \frac{V_2}{2} \exp \left(-r^2 \sqrt{\frac{E_r}{V_1}} \right), \quad (S3)$$

see for instance Refs. [14, 35].

On Fig. S4(a), we plot the critical potential of the second lattice, V_{2c} , versus the amplitude of the first lattice, V_1 , for the imbalanced bichromatic lattice. We find excellent agreement between the results found for the continuous model (solid blue lines) and the prediction of the discrete AA model, corresponding to $\Delta = 2J$ [30] (dashed red lines), for $V_1 \gtrsim 8E_r$.

Figure S4(b) shows the same comparison in the opposite situation where lattice 2 is in the tight-binding regime and lattice 1 is weak. In this case, the AA parameters are changed into

$$J \simeq \frac{4E_r r^{1/2}}{\sqrt{\pi}} \left(\frac{V_2}{E_r} \right)^{3/4} \exp \left(-2r^{-1} \sqrt{\frac{V_2}{E_r}} \right) \quad \text{with} \quad \Delta \simeq \frac{V_1}{2} \exp \left(-r^{-1} \sqrt{\frac{E_r}{V_2}} \right). \quad (S4)$$

Then, the critical potential V_{1c} found in the continuous model approaches the AA prediction for $V_2 \gtrsim 6E_r$.

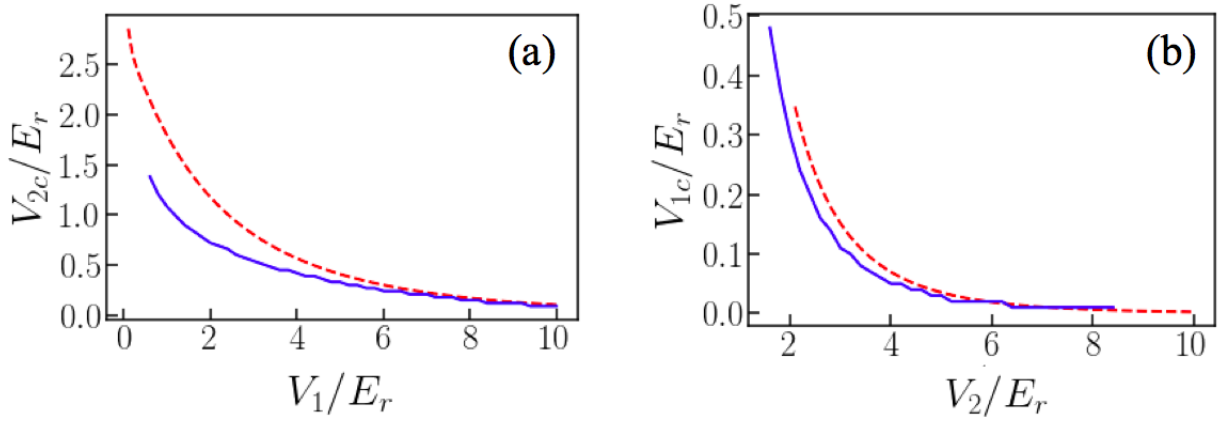


Figure S4. Comparison between the critical point found in the continuous bichromatic model (solid blue lines) and the discrete Aubry-André model (dashed red lines). Panel (a) corresponds to the tight-binding regime for lattice 1 and panel (b) to tight-binding regime for lattice 2, respectively.

Finally, we illustrate here the difference between the IPR and the Lyapunov exponent as probes of localization. On Fig. S5, we plot the ground-state wavefunction for the AA model slightly above the critical point, namely $\Delta/J = 2.05$. The wavefunction shows a clear exponential localization in the wings. The dashed red lines are the fitted exponential function $|\psi| = e^{-\gamma|x-x_0|}$ with the localization center x_0 and the Lyapunov exponent γ . It yields $\gamma = 6.20 \times 10^{-3} \pm 6.85 \times 10^{-5}$. However, the wavefunction is not a pure exponential functions. In particular, it shows a core about one order of magnitude larger than the exponential fit at the localization center x_0 . This core dominates the IPR. For instance, computing the IPR, restricting the wavefunction to the range $[x_1, x_2]$ such that $\psi(x_1) = \psi(x_2) = 0.01\psi(x_0)$, 99.5% of the value found for the full wavefunction. Therefore, the IPR is independent of the exponential behaviour of the tails, and the IPR and Lyapunov exponent yield different information about localization. In particular, they are characterized by different critical exponents at the critical point $\Delta = 2J$: We find

$$\text{IPR}_0 \sim (V_2 - V_{2c})^\nu \quad \text{and} \quad \gamma \sim (V_2 - V_{2c})^\beta, \quad (\text{S5})$$

with $\nu \simeq 0.33 \pm 0.015$ and $\beta \simeq 0.96 \pm 0.04$.

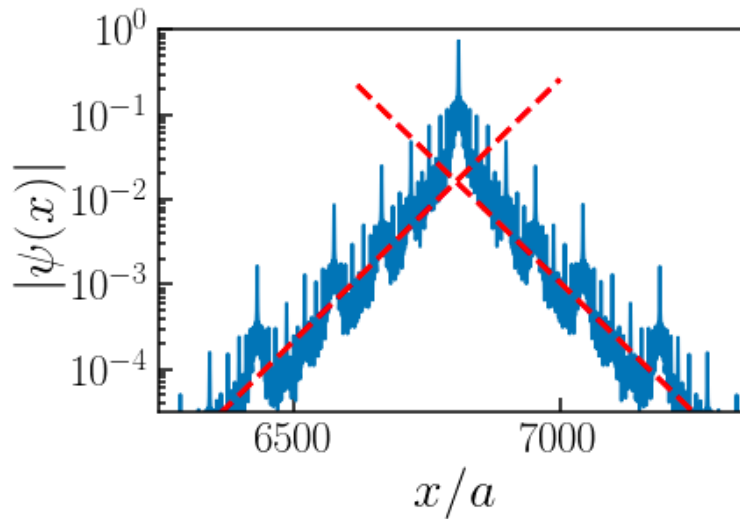


Figure S5. Ground-state wavefunction of the Aubry-André model for $\Delta/J = 2.05$ (solid blue line) together with exponential fits (dashed red lines) on the left-hand and right-hand sides of the localization center.